A Search for Distant Galactic Cepheids Toward $\ell = 60^\circ$[1]

Mark R. Metzger[2,3] and Paul L. Schechter
Physics Department, Room 6-216, Massachusetts Institute of Technology,
Cambridge, MA 02139
mrm@grus.caltech.edu, schech@achernar.mit.edu

ABSTRACT

We present results of a survey of a 6-square-degree region near $\ell = 60^\circ$, $b = 0^\circ$ to search for distant Milky Way Cepheids. Few MW Cepheids are known at distances $\gtrsim R_0$, limiting large-scale MW disk models derived from Cepheid kinematics; this work was designed to find a sample of distant Cepheids for use in such models. The survey was conducted in the V and I bands over 8 epochs, to a limiting $I \simeq 18$, with a total of almost 5 million photometric observations of over 1 million stars. We present a catalog of 578 high-amplitude variables discovered in this field. Cepheid candidates were selected from this catalog on the basis of variability and color change, and observed again the following season. We confirm 10 of these candidates as Cepheids with periods from 4 to 8 days, most at distances > 3 kpc. Many of the Cepheids are heavily reddened by intervening dust, some with implied extinction $A_V > 10$ mag. With a future addition of infrared photometry and radial velocities, these stars alone can provide a constraint on R_0 to 8%, and in conjunction with other known Cepheids should provide good estimates of the global disk potential ellipticity.

Subject headings: Cepheids — Galaxy: fundamental parameters — Galaxy: stellar content — Galaxy: structure — distance scale — techniques: photometric — surveys

1. Introduction

Analysis of the kinematics of classical Cepheids in the disk of the Milky Way has provided one of the most accurate means of measuring fundamental parameters of the Galactic disk potential. Since its first application by Joy (1939), the catalogs of known Cepheids have grown and included

[1]Based in part on observations using the 1.3m McGraw-Hill telescope at the Michigan-Dartmouth-MIT Observatory

[2]Present Address: California Institute of Technology, Astronomy 105-24, Pasadena, CA 91125

[3]Visiting Astronomer, Kitt Peak National Observatory. KPNO is operated by AURA, Inc. under contract to the National Science Foundation.

increasingly higher quality data. Recent measurements of fundamental parameters such as the distance to the Galactic center, R_0, and the local circular rotation speed v_{circ}, have yielded estimates to better than 5% given certain model assumptions (Pont, Mayor, & Burki 1994a; Metzger, Caldwell, & Schechter 1997, hereafter MCS).

The distribution of known Cepheids in the Galactic disk, however, is quite lopsided: a large fraction of the known distant Cepheids, and hence most of the leverage in determining R_0 from kinematic models, lies in the region $270^\circ < \ell < 360^\circ$ (in the southern hemisphere). MCS showed that by adding only eight well-placed Cepheids to the models, the uncertainty in the measurement of R_0 could be significantly reduced, and most of the weight in the distance measurement rested on the new Cepheids. A peculiarity in the properties of the region containing most of the new Cepheids not taken into account by the models (such as a streaming motion, unusual dust properties, etc.) might systematically skew the estimate of R_0. To confirm the distance measurements and test the validity of the model assumptions, one would like to obtain additional Cepheids with good R_0 leverage in other regions of the disk.

One source of systematic uncertainty in kinematic measurements of R_0 is a possible large-scale deviation of the true rotation curve from axisymmetry (e.g. Blitz & Spergel 1991; Kuijken & Tremaine 1994); many traditional kinematic models have assumed axisymmetry. MCS found that the existing Cepheid sample is inadequate for measuring many deviations from axisymmetry, and suggested a two-pronged strategy to extend the sample so that each of two ellipticity components could be measured directly. To address the issue of obtaining additional Cepheids to help reinforce our measurement of R_0, and to provide additional constraints on the rotation curve ellipticity, we undertook a survey for Cepheids toward $\ell = 60^\circ, b = 0^\circ$ where few distant Cepheids were known. The survey is similar in many respects to the one conducted in the southern hemisphere by Caldwell, Keane, and Schechter (1991, hereafter CKS), and the design of this survey is based in part on lessons learned from the CKS survey. Wide-area surveys requiring accurate photometry of a large number of stars have only recently become possible due to the availability of large charge-coupled device cameras. The new CCDs cover a large area of sky while providing enough spatial resolution to allow accurate photometry, even in the crowded fields associated with the Galactic plane.

At the time the survey was proposed, one of the best facilities available was the KPNO 0.9m telescope/Tektronix 2048^2 CCD combination: this configuration can cover a square degree in seven pointings with 0.7 arcsecond sampling. We had initially started a survey during summer shutdown at the McGraw-Hill 1.3m telescope at MDM Observatory, but the only detector then available covered an area of sky 20 times smaller and thus limited the survey to an insufficient total area. Even with the high efficiency of the 0.9m telescope, however, only a limited area of the Galactic plane can be covered in a single observing run. We therefore took some care in the design of the survey to maximize the payoff for Galactic structure study.

2. Survey Design

Cepheids that contribute weight to both a more precise measurement of R_0 and global rotation curve shape lie at distances of several kiloparsecs ($\gtrsim 0.5R_0$). Given a fixed accuracy in measuring distances to the tracers, Schechter *et al.* (1992) found that for stars lying near the solar circle, the uncertainty in $\log R_0$ caused by the intrinsic velocity dispersion of the tracer (~ 10 km s^{-1} in the disk for Cepheids) is minimized in the northern Milky Way toward $\ell \sim 35°$. Cepheids that lie on the solar "circle" (rotating at the same angular speed) have the additional advantage of constraining R_0 independently of the rotation speed. Unfortunately, extinction to these stars due to dust can be quite large: they lie at a distance of over $1.7R_0$, and the line of sight passes within $0.6R_0$ of the Galactic center. Further, measuring an asymmetry in the rotation curve is much simplified by having tracers symmetric about the Galactic center. We therefore chose to conduct the survey near $\ell = 60°$ where few distant Cepheids are known, reducing the total extinction and complementing the CKS survey toward $\ell = 300°$.

Limits on the survey latitude can be set based on the measured distribution of local Cepheids, which have a scale height of 70 pc (Kraft & Schmidt 1963). At a distance of R_0 this corresponds to roughly $0\overset{\circ}{.}5$, thus to find Cepheids at a distance of R_0 we should focus on areas with $|b| < 0\overset{\circ}{.}5$. Indeed, of the Cepheids discovered in the CKS survey, all but one were within this latitude range. One might argue that since the extinction close to the plane is very high, we should avoid $b = 0°$ and look slightly away, improving the depth of our survey. Unfortunately the dust is unavoidable: the vertical scale height of Cepheids is similar to that of dust, and so to reach distant Cepheids one must necessarily look through the dust as well. If one moves out of the plane, the integrated dust decreases, but the survey becomes less efficient as the Cepheid density drops as well.

The distribution of dust is not uniform, however, so one can hope to gain an advantage by choosing lines of sight having relatively low extinction. CKS were fortunate to take advantage of one of the least heavily reddened lines of sight in the inner Galaxy; no comparable region exists near $\ell = 60°$. We can nonetheless use existing survey data to provide an idea of which areas have lower extinction, and give these areas priority in our Cepheid survey. One method of estimating extinction is to compare the faint source counts (or total source flux) in different regions. Since the stellar luminosity function $\Phi(M)$ is shallower than an $n = 3/5$ power law, the number of faint sources will decrease dramatically as the extinction increases. Surveys at optical wavelengths (e.g. the Palomar Observatory Sky Survey), however, provide little information on dust at a distance, as the counts are dominated by stars closer than the Cepheids we seek, particularly if the total extinction is large.

Near-infrared surface brightness maps are more useful in this regard. The extinction is significantly reduced at these wavelengths, and thus the surface brightness will have a greater contribution from stars at large distances. The surface brightness variations (after subtracting a smooth Galactic component, which varies with longitude) are thus more closely correlated to the extinction out to many kiloparsecs. To help select regions of interest, we examined data from

the Spacelab IRT 2μm survey of the Galactic plane (Kent *et al.* 1992), which has an effective resolution of about 1 degree. Figure 1 shows a plot of flux integrated over $|b| < 0.^\circ 5$ as a function of longitude. Most of the structure appears on scales larger than the effective resolution, relieving some concern about contamination from bright point sources.

Regions of potentially low extinction can also be mapped using data on molecular CO emission. The distributions of gas and dust in the Galaxy have been shown to be fairly well correlated (e.g. Hilditch, Hill, & Barnes 1976; Burstein & Heiles 1978, Heiles, Kulkarni, & Stark 1981); CO is a particularly good tracer of dust as both tend to survive under similar physical conditions. We examined data from the survey of Dame *et al.* (1987) to generate column densities of CO gas as a function of longitude in a 2-degree-wide band at the plane, shown in Figure 2. A further advantage of using gas is that the surveys provide column densities in narrow bands of velocity (1.3 km s^{-1} in the Dame *et al.* survey), allowing us to select the depth to which we measure the density. Since all of the gas on the near side of the solar circle has positive rotational velocity with respect to the LSR, and more distant gas has negative velocity, by integrating only gas with positive velocity we produce a total CO column density out to the solar circle. This provides a better indication of the total extinction between the Sun and the more interesting Cepheids. Several features can be seen in common between the near-infrared and CO maps: as an example, the strong 2μ emission near $\ell = 68^\circ$ corresponds to a local minimum of CO column density, precisely what we would expect if this feature were caused by differential extinction.

Using a combination of these two data sets we assigned a relative priority to different areas along the Galactic plane in the vicinity of $\ell = 60^\circ$, $b = 0^\circ$. We divided this region of the plane into 98 regions of 1300 arcseconds square with borders aligned north-south. This is the size and orientation of the Tektronix CCD on the KPNO 0.9m telescope, allowing for a small overlap between regions (see §3). A list of the regions with numeric designations and coordinates is given in Table 1.

2.1. Cepheid Detection

In addition to selecting areas of the plane with relatively low obscuration, we can conduct the survey at wavelengths that have lower total extinction. A longer-wavelength band such as I ($\sim$ 800 nm) gives only about 60% of the extinction in *magnitudes* than suffered at V ($\sim$ 530 nm), and less than half that of B ($\sim$ 420 nm) (see, e.g., Clayton, Cardelli, & Mathis 1989). While the situation improves even more at longer wavelengths, the existing detectors become significantly smaller: for surveys in the K-band (2.2 μm) the largest available detectors had sky dimensions 5 times smaller (and at poorer resolution) than the large optical CCDs, which would reduce the survey efficiency by a factor of over 20. Another competing factor is the pulsation amplitude, which is significantly larger at blue wavelengths ($\sim$ 1.2 mag at B) than in I ($\sim$ 0.4 mag; Madore & Freedman 1991) or K ($\sim$ 0.1 mag; McGonegal *et al.* 1983). Even so, the extra amplitude does not help to find less heavily reddened Cepheids, where the photometric accuracy in I is more than sufficient to

detect pulsation. For more heavily-reddened stars the flux in bluer bands drops dramatically, and requires very long exposures even to recover the objects. The best detection sensitivity over a wide range of distance and extinction is therefore obtained in the reddest bands we can use. For optical CCDs this is the I-band, and therefore we followed CKS in choosing the I band for the primary survey.

The effects of extinction make dynamic range a particularly important issue. In the absence of extinction, the apparent brightness of a star at $0.1R_0$ and one at $1.0R_0$ differ by a factor of 100. However, it would not be unreasonable to encounter 5 magnitudes of extinction at I over $0.9R_0$ (7 kpc) in the inner galaxy, making the distant cousin appear 10,000 times fainter. The exposure times were therefore chosen to reach as faint as possible, while attempting to keep nearby bright Cepheids under saturation. All but one of the Cepheids discovered in the CKS survey were fainter than 11th magnitude in I, typically with 2 or more magnitudes of extinction. To make our bright end cutoff, we tried to insure that we would recover a 10-day period Cepheid at a minimum distance of $0.3R_0$ under 2 magnitudes of extinction in I. Thus we set our exposures to a maximum time that will place a star of I = 10.5 mag at the saturation limit, which was quoted as 240,000 photoelectrons pixel^{-1} for the Tektronix CCD. Cepheids much brighter than this would likely have been discovered previously, given the distribution of known Cepheid magnitudes (Kholopov *et al.* 1988); the faintest known Cepheid in our survey region, GX Sge, has $\langle V \rangle = 12.4$ and $I \simeq 10.3$.

One significant difference between this survey and that of CKS was the decision to obtain data in the V band for each field at several epochs. This was motivated by the realization that the characteristic pattern of color change of a Cepheid over its pulsation cycle is a powerful way to distinguish Cepheids from other types of variable stars. In the CKS survey, stars were selected for follow-up photometry without the benefit of knowing the color change. If one were to have this information a priori, many variable stars could be eliminated before followup photometry was conducted, and a larger sample of promising candidates could therefore be examined. However, if V frames are observed throughout the survey, the total area covered would be cut in half (the V exposures would have to be at least as long as those in I). The compromise was to observe V in each field for every three I observations, providing a reasonable chance of measuring a color change (which requires at least two points) while reducing sky coverage by only one quarter.

Another issue is the distribution of individual observations over time. Identifying a Cepheid requires both detecting its variability at a sufficient confidence level and recognizing it as a Cepheid from the properties of its light curve (such as a fast rise/slow decline, color change, etc.) While better sampling provides more information on the light curve shape, CKS showed that 7 epochs of observations were sufficient to recognize a Cepheid, assuming coverage spaced over the entire cycle. Cepheids range in period roughly between 3 and 70 days, and the number distribution is heavily skewed towards shorter periods (Feast & Walker 1987). To obtain reasonable phase coverage of longer period Cepheids, the baseline (number of days between the first and last observation) should be as long as possible, and observations must be made frequently enough to sample the short-period Cepheids. In practice the latter criterion is met without difficulty, as

one can observe each field once per night or on every other night. The solution we chose was to observe each field once per night for four nights, pause for four nights, and observe again for four nights. This provides a baseline of 11 days, which should allow detection of Cepheids with up to 22 day periods (§5) while providing adequate phase coverage for shorter-period Cepheids. The allocated time was broken into three nights on, two nights off, and five nights on, which lowered slightly our sensitivity to long-period Cepheids.

3. Observations

Observations for the survey were taken with the 0.9m telescope at Kitt Peak National Observatory on the nights of June 9–11 and 13–18, 1992, using a Tektronix 2048^2 CCD. The detector scale was 0.69 arcseconds per pixel, giving a field of ≈ 23.5 arcminutes square (0.15 square degrees). The regions observed each night and the filters used are listed in Table 2. We were able to cover a total area of approximately 6 square degrees over a single night. The observing efficiency was limited primarily by the readout time of the chip and the rate at which the telescope could be moved between fields; a faster readout, automated repositioning, or possibly scanning along the plane might have improved observing efficiency. Figure 3 shows a star map made using the HST Guide Star Catalog (Lasker *et al.* 1990, hereafter GSC), with some of the surveyed regions outlined. Clouds prevented us from observing for part of night 6 (June 15) and all of night 9 (June 18). When telescope hardware problems occurred on two nights that limited the amount of usable observing time, first priority was given to acquiring the full set of I observations; for this reason no V observations were taken on night 2.

Exposure times were typically 40 s for I and 60 s for V, but were increased during periods of poor seeing to compensate for the effective increase in noise (and due to the reduced danger of saturating bright stars). The V filter used was a glass filter from the Kitt Peak "Harris" set, the I was an interference filter. Traces of the filter response curves are given by Schoening *et al.* (1991). Photometric standards of Landolt (1992) and Christian *et al.* (1985) were observed at the beginning and end of each night when possible. Images of both the twilight sky and an illuminated dome spot were taken each night in both filters to allow correction of the detector response to an even illumination level.

A significant problem with the images was the variation of the point spread function across the chip. The telescope focal plane was not flat with respect to the CCD, which caused the focus to vary from the center to the edge. The astigmatism (and, as apparent from the images, some coma) present in the optics produced out-of-focus images that were elongated in the NW-SE direction on one side of focus, and NE-SW on the other side. If the focus was properly adjusted at the center of the chip, the images at the corners were significantly distorted. Figure 4 shows the point spread function near the center and corner of the chip. Each plot is a composite of 10 stars, created by subpixelizing, interpolating, centroiding on the peak, and co-adding a region around each star. The contours shown are logarithmic at $\sqrt{2}$ intervals; the third contour from

the center is the half-maximum. The image distortions are particularly troublesome as they constantly change: as the temperature varies through the night, the focus drifts and has to be re-adjusted. Between corrections, however, the PSF will shift shape as the focus shifts, with most areas typically becoming more elongated. Even if the focus could be tracked perfectly, the relative contribution of the astigmatism to the PSF shape is a function of the atmospheric seeing, which also varies throughout the run.

The PSF variation across the chip required some extra care in the data reduction, as described below. During the observing run, we attempted to reduce the problem slightly by setting the focus at a compromise position, where images in a ring around the center were in focus, the center slightly outside focus, and the corners somewhat inside focus. The field curvature problem has since been remedied at the 0.9m telescope with the installation of a corrector lens in the summer of 1993.

4. Data Reduction

The bias from each image was computed from a serial overclock region and subtracted, then the images were corrected for variations in sensitivity using composite twilight flats; separate composite flats were constructed for each night. Some systematic variation was evident between the individual flats, but it remained $< 0.5\%$ throughout. We compared the use of dome vs. twilight flats to correct the data, and found that the CCD illumination was quite different between the two. By comparing the flats to data images with high night sky levels or images of a globular cluster, M92, taken at many different positions on the chip, we found the twilight flats corrected the detector response quite well. We concluded that the dome flats suffered from an uneven illumination problem, and were therefore discarded.

Stars were identified and measured in each of the images using a modified version of the photometry program DoPHOT (Schechter, Mateo, & Saha 1993). DoPHOT fits each star to an intensity profile of the form

$$I(x,y) = I_0\left(1 + z^2 + \frac{\beta_4}{2}z^4 + \frac{\beta_6}{2}z^6\right)^{-1}, \tag{1}$$

$$z^2 = \frac{1}{2}\left(\frac{x^2}{\sigma_x^2} + 2\sigma_{xy}xy + \frac{y^2}{\sigma_y^2}\right); \tag{2}$$

where the shape parameters β_4 and β_6 are held fixed, and the other shape parameters σ_x, σ_y, and σ_{xy} are allowed to vary when fitting the profile to individual bright stars. The standard DoPHOT algorithm computes an average shape for the stars in the image using the means of σ_x, σ_y, and σ_{xy}. This average shape is used in fitting each star to measure the flux, and typically provides a better flux estimate than if the shape parameters were allowed to vary independently.

This algorithm assumes that the PSF is constant; if the PSF varies across the chip, the average PSF will not fit any of the stars well, introducing additional photometric error. Worse,

the PSF at the edge of the chip shown in Figure 4 is so elongated that it fits better to *two* average PSFs than one, and DoPHOT will happily split every star in the corner into two components. We therefore modified the standard DoPHOT algorithm, to allow the average shape of the point spread function to vary as a function of position on the chip. Rather than taking a straight average for PSF shape parameters, we fit a second order two-dimensional polynomial for each shape parameter as a function of position. The flux for each star was obtained by fitting a PSF using the shape parameters $\sigma_x(x_0, y_0)$, $\sigma_y(x_0, y_0)$, and $\sigma_{xy}(x_0, y_0)$ obtained from the 3 independent fit functions. The parameters β_4 and β_6 were fixed at 1.0 and 0.5, respectively.

The second-order polynomial fit for the shape parameters turned out to be insufficient to match the PSF variation across the entire chip. A better match was obtained by breaking up a single 2048^2 image into five 1124^2 tiles (four quadrants plus an overlapping center), fitting the roughly monotonic PSF variation in each quadrant separately. After fitting for positions and fluxes for each star, the catalogs of the individual quadrant "tiles" were combined into a single catalog. The center tile was used as a reference, and each corner quadrant's overlapping stars were matched to the reference. A mean magnitude offset computed from these stars was applied to each corner tile, to keep the relative photometric system commensurate between tiles. This correction was small, typically 0.005 mag and not exceeding 0.013 mag.

4.1. Catalog Construction

To match stars between different observational epochs, the centroid positions of ~ 200 bright stars per field were computed and cross-referenced between fields. A transformation consisting of an (x,y) offset and a linear 2x2 matrix was computed from the coordinates, and the transformation was used to map the remaining stars to the reference template. The data of night 2 was used as the initial template, as it had the best average seeing. Two objects were considered a potential match if a box 3 pixels (~ 2") high, centered on the transformed position of the candidate object, included the reference object. If there were no other reference stars in the box, the match was considered good and the offsets in RA and Dec were recorded. If there was more than one reference star in the box, the closest star was considered the match and the object was flagged as possibly confused ("type b" confusion). If, however, the best match reference object for a candidate was also the best match for another candidate, both candidates are labeled as confused ("type a" confusion), and the candidate closest to the reference object is considered the match. If a candidate object has no match on the reference frame, it is added to the reference catalog for subsequent use.

After the initial matches were made, a complete reference catalog was produced using the mean position for each object, and the matching procedure was repeated. The scatter in stellar positions between fields taken on different nights was typically 0.15 pixels rms, or ~ 0.1 arcseconds, in each coordinate. The number of confused objects was a strong function of the field crowding, as expected: the least crowded fields, with $\sim 12,000$ identified objects, typically had 20 confused

objects; the most crowded fields had over 40,000 objects with roughly 300 confused.

In a survey searching for variability it is crucial to ensure that the observations at different epochs are on the same *relative* photometric system. We therefore used stars in the field to determine a mean relative magnitude offset at each epoch. Since the skies on night 2 were closest to being photometric (as judged from the standard field analysis), all epochs were transformed to the night 2 system. Of the stars matched to the reference frame, the brightest 5% (to avoid non-linearity) and faintest 20% (large scatter) of the stars were eliminated, and the rest used to derive a mean magnitude offset. Stars deviating form this mean by more than 5σ were eliminated (such stars are likely variable), and a final mean offset was computed and applied to the field stars to bring them onto the reference photometric system.

It was found, however, out that a simple average was not sufficient to bring the two frames into good relative calibration, as the variation of the PSF produced errors ≥ 0.05 mag across the chip. Most of this effect was apparently cause by our use of a single offset to transform DoPHOT fit magnitudes to an aperture system, which is not strictly valid if the PSF shape varies across the chip. Another contribution comes from a systematic difference between the aperture magnitudes for the distorted and normal PSF. To allow for this, we fitted a second order two-dimensional polynomial to the (aperture – fit) magnitudes as a function of position for night 2, and used this to correct the magnitudes to full aperture. The relative calibration between night 2 and other nights was likewise computed from a two-dimensional polynomial. The data was thereby brought to a consistent system that could be directly calibrated to standard magnitudes. The effectiveness of the procedure can be seen both from the formal error of the offset, $\simeq 0.005$ magnitude, and by measuring $\chi^2_\nu \simeq 1.0$ for the bright stars (the bright stars have small formal errors in instrumental magnitude, and thus can be a sensitive test for calibration errors). The locations of variable stars are also close to uniform, as shown below in Figure 8, though from the excess number of variables it is evident that the applied correction was insufficient in one corner.

Figure 5 shows the photometric errors as a function of I magnitude, computed from the scatter of non-variable stars over the course of the survey. Note that the error bottoms out near 0.016 mag, which is likely due to residuals from our polynomial fit calibration; for comparison, the formal error at $I = 11.5$ is 0.013 magnitude. Also note the rise in error brighter than $I = 11$–this is reflected in both the statistical dispersion and the formal errors from DoPHOT, and is caused by charge levels nearing saturation on the detector in nights of good seeing. While we had initially designed the survey to avoid this effect down to $I = 10.5$, the detector nonlinearity extended down to levels lower than the instrument specifications due to changes in the electronics to improve readout speed (R. Reed, private communication).

The instrumental I band magnitudes from night 2 were converted to the standard system of Landolt (1992) using exposures of several fields at the beginning and end of the night. Corrections were made for an absolute offset and an airmass term, but no color corrections were applied. Since many of the stars in our survey are too faint to be detected in the V band, and thus have

no color information, we chose to keep the magnitudes homogeneous and forego a color correction. All magnitudes reported in this section are therefore on an instrumental magnitude system. The color corrections required to convert to a standard system are fairly small, at least over the color range $0 < (B - V) < 2.0$ (see §5.1).

Since we do not have V-band data for each region on all nights, the offset to the standard magnitude system was computed separately for each night. Light to moderate cirrus obscured our observations on several nights, and thus our absolute calibration is less well determined for V than for I. We can get an idea of how bad the cloud extinction was by looking at the I-band data taken shortly before or after a V image. With the exception of night 6, when the clouds increased steadily until it was no longer possible to observe, the total extinction from clouds in I was < 0.07 mag at all times. The absolute calibrations in V therefore should be accurate to ~ 0.10 mag. The photometry of §5.1 supports this assessment: for the fields that overlap the follow-up area, the absolute calibrations agree to better than 0.05 mag. For the purposes of identifying Cepheids, the V photometry is important primarily to measure the color change, which is not dependent on an accurate absolute calibration. More accurate V magnitudes for the Cepheids were then obtained during followup.

Coordinates in equinox J2000 were determined by matching stars in the survey regions with stars in the GSC in the same manner as we matched the survey data. This produces a coordinate transformation from which we can calculate RA and Dec from the centroid position in pixel coordinates. Each region had between 19 and 182 GSC stars, enough to provide a solution good to the accuracy of the catalog (~ 1" quoted error, probably somewhat higher near GSC plate edges).

We initially tried the approach used by CKS to match survey objects, first by transforming to sky coordinates and performing the match based upon true sky distances. We found, however, that errors in star positions near the edges of the GSC survey plates introduced spurious errors into the coordinate transformations. We therefore chose to match objects in pixel coordinates; those objects in overlap regions are matched using the same algorithm for *inter*-region matching as used above when re-assembling subregions *intra*-region.

4.2. The Catalogs

The complete survey catalog consists of 4,988,434 photometric measurements of 1,063,515 stars in an area of roughly 6.1 square degrees. Of these stars, 766,816 were detected on three or more nights, and are examined for variability in §5. Figure 6 shows the number distribution of catalog stars as a function of apparent magnitude. The distribution resembles a power law in number vs. flux, and as expected the slope is somewhat shallower than the dust-free value of 3/5. The completeness begins to fall off for stars of $I \gtrsim 17.5$ and those brighter than $I = 11$, assuming the validity of extrapolating the power law a small amount at each end.

Figure 7 shows color-magnitude diagrams of three survey regions covering the middle and

two extremes of ℓ in the survey area. Not all stars from each region have been plotted, to relieve crowding in the plot for region 38; the same fraction of stars is shown for each. Note the progression to redder colors and fewer identified stars with decreasing longitude: only 1,735 stars were identified in both V and I in region 84 ($\ell = 53°$), while region 38 ($\ell = 67°$) boasts almost 15,000. A comparison of the color-magnitude diagrams shows that most of the difference is due to extinction, which shifts a large number of main sequence stars below the flux limit.

5. Variable Stars and Cepheid Candidates

The catalog stars were tested for variability by using the formal errors from DoPHOT to determine a χ^2 value for each star, under the assumption that it does not vary. The criteria for flagging a star as variable were that it have at least 3 photometric measurements, and that the probability of exceeding χ^2 if it were not variable, $P(< \chi^2) < 10^{-4}$; this is similar to the algorithm used by CKS. Out of the roughly 765,000 stars in the catalog having three or more measurements, 7,821 were found to be variable. Some of these variable stars will be spurious: about 1% due to the χ^2 statistics alone. There are also a higher number of variables found among survey stars near one corner of the chip, most likely due to the inability to completely compensate for the systematic offset in photometry. Figure 8 shows the location on the detector where each variable star appeared in the survey; in the absence of irregularities, the distribution should be uniform. Aside from the corner, there is a small patch with an anomalously large number of variables. This is near a location of low intrinsic response on the detector, which we can compensate for properly only if the detector maintains a linear response in that region. Slightly nonlinear response leads to errors in the photometric calibration, and could produce the spurious excess of variables seen.

Further criteria were placed on the variable star catalog to extract a subset having a sufficiently high variability amplitude to potentially be a Cepheid. The typical amplitude of a Cepheid in I is about 0.4 magnitude peak-to-peak; if we approximate a Cepheid by a continuous sine function, we can calculate the RMS variability amplitude expected of a Cepheid as follows. For a full cycle we have

$$\sigma_I^2 = \frac{\int_0^{2\pi} \sin^2 x dx}{\int_0^{2\pi} dx} \frac{A^2}{4} = 0.125\, A^2\,;$$

for a Cepheid observed over the first half of the cycle we find

$$\sigma_I^2 = \frac{\int_0^{\pi} \left(\sin x - \frac{2}{\pi}\right)^2 dx}{\int_0^{\pi} dx} \frac{A^2}{4} = 0.024\, A^2\,.$$

A Cepheid will therefore have $\sigma_I \simeq 0.14$ mag observed over a full cycle and 0.06 mag over one half cycle. We therefore adopted a lower limit of 0.06 mag for the RMS variability in I, to catch the longest period Cepheids, and a further criterion of $P(< \chi^2) < 10^{-14}$ to eliminate spurious candidates. The final selection criterion is that the star must still qualify as a variable star ($P(< \chi^2) < 10^{-4}$) after any single point in the light curve is removed. Strong single-point eclipsers

are thus eliminated from further consideration. The resulting catalog of high-amplitude variables contains 578 stars, and is presented in Table 3.

The number of high-amplitude variables based upon the above criteria is too large to readily acquire additional photometry or spectra for each candidate. As a further selection criterion, if a candidate's color change was 3σ inconsistent with a dV/dI slope of 1.5, it was excluded. This removed about 200 of the candidates, though a large fraction of the candidates do not have color information (see Table 3) so this criterion could not be used. The final selection was made by visually inspecting light curves for each variable. Stars showing light curves inconsistent with a Cepheid's were eliminated, primarily if the amplitude was too high or the rise time was much slower than the decline. Light curves were independently evaluated by the authors in a double-blind fashion. In cases where there was disagreement as to the promise of a candidate, we tried to be inclusive. In the end, the list of candidates was cut to 40 of the most promising stars, for which we could perform follow-up photometry in a single observing run. Other stars not included may still be proven to be Cepheids in the future.

Stars selected for follow-up photometry are indicated in Table 3. The "B" team candidates—a second set that looked promising but which we were unable to observe—are also indicated in the table, and are worthy of further photometry. Stars that were classified as high-amplitude variables and showed a monotonic increase or decrease in brightness are also noted in the table. Most are likely late-type long period variables. Some may be long-period Cepheids, but direct follow-up photometry was not performed; future spectroscopy could help to differentiate the Cepheids without requiring multiple epochs.

Most of the variable stars from the General Catalog of Variable Stars, 4th Edition (Kholopov *et al.* 1988, hereafter GCVS) in our survey area were recovered, including GU Vul (W UMa-type), EW Vul (RR Lyr), KN Vul (W UMa), V1023 Cyg (Algol), and GX Sge (δ Cep). A known Cepheid with $<I> = 10.2$, GX Sge was at the bright end of our survey limit and was barely recovered (on two of the nights with the best seeing, it had saturated the detector). We found it 1 arcminute away from its reported position in the GCVS, a much larger offset than the catalog coordinate precision, but otherwise matching in magnitude and period. We measure GX Sge at RA 19h 31m 10.5s, Dec +19° 15' 25" (J2000). Other GCVS stars recovered were found at the published locations to within quoted uncertainties. The GCVS stars not recovered included V1022 Cyg, a semi-regular variable with a period of 60 days, which is slightly too bright at I to be recovered in the survey; GK Vul, a semi-regular with no listed period, possibly too long for the variability to be detected in this survey; and CQ Vul, a slow irregular variable.

5.1. Follow-up Photometry

Additional photometry of the best Cepheid candidates was obtained on the nights of May 28–June 7, 1993 at the 1.3 m McGraw-Hill telescope of the Michigan-Dartmouth-MIT Observatory.

Images were obtained in both V and I bands using a Tektronix 1024^2 CCD ("Charlotte"; see Metzger, Tonry, & Luppino 1993 for a general description of the MDM CCD systems). The CCD and filters used were similar to the ones used for the main survey: in both cases the CCD used was thinned with 24μ pixels, and the I filter was the same type of interference filter used a year earlier. The pixel size was 0.″51, which meant that under the best seeing conditions (0.″9) our images were slightly undersampled. Conditions were photometric on several nights, allowing us to improve the absolute calibration for the Cepheids over the original survey data. Twilight sky flat-field images were taken each night, and photometric standards of Landolt (1992) were taken frequently at multiple zenith angles to allow a correction for atmospheric extinction. Each frame was corrected for variations in detector response and throughput using composite twilight flats, one composite for each night. From one night to another and over a range of exposure levels, the corrected response was linear to $< 0.3\%$, except for a 0.6% difference before and after a thermal cycle of the dewar.

Instrumental magnitudes were measured using apertures 3.″5 in diameter, and corrected to an effective magnitude for a 10" diameter aperture using isolated bright stars in the images. Instrumental magnitudes were measured for the standards in the same manner, and used to determine atmospheric extinction coefficients and color corrections to a standard magnitude system. The transformations are given by

$$I = m^i_{1\mathrm{e}} + 23.253(10) - 0.121(20)[\sec z - 1.0] + 0.017(8)[V - I]$$

and

$$V = m^v_{1\mathrm{e}} + 23.683(10) - 0.215(19)[\sec z - 1.0] - 0.014(7)[V - I]\,,$$

where $m^b_{1e} = -2.5\log_{10}(f^b)$, f^b is the corrected 10" flux in $\mathrm{e}^-\ \mathrm{s}^{-1}$. Colors of standards used to compute these relations were in the range $-0.21 < (V - I) < 1.76$ and were linear to within the errors. Most of our target stars are outside this range, therefore we have extrapolated this relation to all colors. Such an extrapolation is uncertain, however, and should be viewed with caution. Fortunately the color terms are small, and we expect that for $(V - I) < 3.5$ the uncertainty should be smaller than the typical photometric error for all but the brightest stars.

5.2. New Cepheids

Of the 31 stars observed, 10 are confirmed to be Cepheids, with one additional star likely to be a Cepheid but with an unusual color variation. Table 4 shows a summary of the data, and Figures 10–12 show I light curves and V vs. I color data for the newly-discovered Cepheids. Of the remaining stars, most had no identifiable periodicity when combined with the original survey data, down to a period of about 2 days; others appeared periodic but did not have the appropriate color change for a Cepheid ($dV/dI \gtrsim 1.3$; Madore & Freedman 1991, Avruch 1991). The candidate 19450+2400 exhibited clearly periodic behavior with a long period, and $dV/dI = 1.45$, but the light curve was too sinusoidal for a Cepheid of that period.

One candidate star (19508+2620) appeared to have a slope of color change too shallow to be a Cepheid. Under close examination of a V image taken in good seeing, however, we discovered a neighboring star close to the candidate that was roughly equal in brightness to the Cepheid at minimum light. The V photometry was contaminated with the light from this star, which caused the V amplitude to appear shallower and thereby affected the slope of the color change. The I light curve is not significantly affected as the Cepheid is much brighter in I (due to its relatively red [V–I]= 3.8). Since this is an effect of roughly 0.4 magnitudes at V, the overall slope in V if this star were not present would be ~ 1.6, in line with what we expect for a Cepheid. Since the I light curve is also clearly consistent with that of a Cepheid, we are confident that this star is properly classified as such. Another candidate, 19286+1733, also has a light curve similar to that of a Cepheid but dV/dI too shallow. We were unable to identify a contaminating star in this case, thus we have left its classification as tentative pending spectroscopic observations.

Periods for the Cepheids were determined using the minimum string length method (Burke *et al.* 1970, Dworetsky 1983), in a similar way as for southern hemisphere Cepheids by Avruch (1991). The observations were folded about a particular test period, and a string length is computed by summing distances between points consecutive in phase. A wide range of test periods were searched for each star, and the one having the minimum string length is taken to be the period. In practice this method is quite sensitive to photometric errors, and isn't well suited to occasional outliers. In cases where this is a problem, however, the minimum string length will usually correspond to some period that is clearly discordant, and single points can be deleted and re-fit. Avruch (1991) performed a Monte Carlo analysis of period errors associated with this method, but since we have two sets of observations taken one year apart, our error is dominated by that due to adding or deleting one full cycle between the two observing seasons. It is the one year baseline which gives most of the precision in determining the period: a change in period of roughly 1 part in 70 (1 cycle change over a year for a 5 day period) is not well constrained by data from one year alone, and thus our periods are accurate only to the 1 part in 70 level. To improve the measurement, we would need a third set of observations to remove the ambiguity, at which point periods should be obtainable to better than 1 part in 1000.

6. Discussion

Out of a sample of over 1 million stars in a six square degree area, we have discovered 10 new Cepheid variables with periods ranging from 4 to 8 days. As we expected, the extinction toward these stars is significantly higher than that toward the Cepheids discovered in the CKS survey. There may also be a bias against Cepheids outside the 4–8 day period range, which may have arisen in the qualitative evaluation of the light curves from the survey (which clearly show the light curve shape for periods in this range). The lack of Cepheids with longer periods is likely caused both by being preferentially excluded due to the short baseline in the survey, and that they are intrinsically rarer than shorter period Cepheids.

One of our Cepheids, 19431+2305, is the most heavily reddened Cepheid known to date. While we do not yet have an accurate color for this star, we can barely detect it in a single long V exposure obtained at the 2.4m Hiltner telescope, which gives puts it at approximately (V–I)= 6.3. Assuming an intrinsic color of roughly 0.65 (Madore & Freedman 1991), this implies a total extinction in V, A_V, of roughly 14 magnitudes, using an extinction law appropriate for Cousins I. This places the star at a distance modulus of approximately 12.2, or only 3 kpc. Such an estimate is only approximate, as both the calibration of magnitudes to standard bands and the extinction law are not well determined for stars this heavily reddened. However, preliminary observations in the K-band tend to support the 3 kpc distance estimate. We have hit a limit on the distance of Cepheids that can be identified in an I-band survey of the inner disk; going deeper at typical ground-based seeing results in a significant crowding problem.

The approximate positions of the new Cepheids are shown in Figure 13. An intrinsic color of (V–I) = 0.65 was assumed, and an absolute magnitude calibration of $M_I = -3.06(\log P - 1) - 4.87$) was used to determine distances (Madore & Freedman 1991). Apparent I magnitudes of the stars were de-reddened using the relation $A_I = 1.5E(V - I)$, following the reddening law of Cohen *et al.* (1981). Most of the Cepheids are closer than R_0, though we apparently reached the solar circle at $\ell = 61.2$ and $\ell = 67.4$. The distances are uncertain primarily due to the uncertainty in dereddening the apparent magnitudes. We have also assumed that each star is a classical (Type I) Cepheid, though with the available data we are unable to distinguish them from W Vir stars (Type II Cepheids). The contamination from W Vir stars should be small, however, as they are Population II stars and the survey was confined to the disk.

Based on this crude estimate, we see that most of the new Cepheids lie in regions where none were previously known, and once radial velocities are measured for these stars, they will provide useful constraints on both R_0 and the ellipticity of the rotation curve. Using the relation given by Schechter *et al.* 1992,

$$\frac{dv}{d \ln R_0} = v_o \sin \ell \left[\frac{d^2 - d \cos \ell}{[1 + d^2 - 2d \cos \ell]^{3/2}} \right] ,$$

we find that the most distant Cepheid can by itself provide an estimate of R_0 to 12%, assuming an intrinsic velocity dispersion of 11 km s^{-1} in the disk. The sample of 10 should yield an R_0 measurement with an uncertainty of 8% once radial velocities and accurate distances are measured. When combined with the full sample of known Galactic Cepheids, these stars can be used to directly test the symmetry of the rotation curve about the Galactic center to roughly 5%: current estimates from the new southern hemisphere Cepheids are about 5%, and the measured R_0 can be directly compared in the northern and southern hemispheres.

The high extinction found in the direction of these stars presents two problems. The immediate problem is to measure accurate distances to the newly discovered Cepheids, which can be best accomplished by obtaining photometry in the near-infrared 2.2μ K-band. We have started an observational program to measure these stars, and have obtained data for these and many other accessible Cepheids nearby. The K-band is significantly less affected by extinction and

presents a smaller scatter in the observed PL relation, both leading to more accurate distances than can be obtained optically. Radial velocity measurements are also made more difficult by the high extinction, but might be obtained from high-resolution infrared spectra.

It is also evident from the extinction encountered that future surveys for more distant Cepheids should be conducted in the near infrared. A survey concentrating at K, with additional JH photometry to aid identification and provide reddening estimates, is probably the best strategy for ground-based surveys, particularly for the inner disk. At K wavelengths and longer, the amplitude of variation is roughly 0.3 magnitude, reflecting the change in surface area (Welch *et al.* 1984). Even under the equivalent of 30 magnitudes of extinction in V (approximately the extinction to the Galactic center), a 3-day period Cepheid at a distance of R_0 would have an apparent magnitude of $\sim$13.5 and can easily be measured with the required photometric accuracy for detecting variability. Crowding will become a significant problem, however, and therefore a substantial survey awaits the availability of large-format infrared arrays (e.g., Hodapp et al. 1996) that can simultaneously cover large areas with sufficient angular resolution.

We thank Hal Halbedel for valuable assistance during our observing at Kitt Peak, and Bob Barr for working out innumerable last-minute details at MDM. Thanks also go to Craig Wiegert for his help in acquiring the MDM followup data. This work was supported by NSF grants AST-8996139, AST-9015920, and AST-9215736.

REFERENCES

Avruch, I. M. 1991, M.S. Thesis, Massachusetts Institute of Technology.

Blitz, L., & Spergel, D. N. 1991, ApJ, 370, 205

Burstein, D., & Heiles, C. 1978, ApJ, 225, 40

Caldwell, J. A. R., & Coulson, I. M. 1987, AJ, 93, 1090 (CC)

Caldwell, J. A. R., Keane, M. J., & Schechter, P. L. 1991, AJ, 101, 1763 (CKS)

Caldwell, J., Avruch, I., Metzger, M., Schechter, P., & Keane, M. 1992, in Variable Stars and Galaxies, ed. B. Warner, ASP Conf. Ser. 30, 111.

Christian, C. A., Adams, M., Barnes, J. V., Hayes, D. S., Siegel, M., Butcher, H., & Mould, J. R. 1985, PASP, 97, 363

Clayton, J. A., Cardelli, G. C., & Mathis, J. S. 1989, ApJ, 345, 245

Dame, T. M., Ungerechts, U., Cohen, R. S., de Geus, E. J., Grenier, I. A., May, J., Murphy, D. C., Nyman, L.-Å., & Thaddeus, P. 1987, ApJ, 322, 706

Dworetsky, M. M. 1983, MNRAS, 203, 917

Feast, M. W., & Walker, A. R. 1987, ARA&A, 25, 345

Heiles, C., Kulkarni, S., & Stark, A. A. 1981, ApJ, 247, 73

Hillditch, R. W., Hill, G., & Barnes, J. V. 1976, MNRAS, 176, 175

Hodapp, K.-W., Hora, J. L., Hall, D. N. B., Cowie, L. L., Metzger, M., Irwin, E., Vural, K., Kozlowski, L. J., Cabelli, S. A., Chen, C. Y., Cooper, D. E., Bostrup, G. L., Bailey, R. B., Kleinhans, W. E. 1996, New Ast., 1, 177

Joy, A. H. 1939, ApJ, 89, 356

Kent, S. M., Mink, D., Fazio, G., Koch, D., Melnick, G., Tardiff, A., & Maxson, C. 1992, ApJS, 78, 403

Kholopov, P. N., Samus, N. N., Frolov, M. S., Goranskij, V. P., Gorynya, N. A., Kireeva, N. N., Kukarkina, N. P., Kurochkin, N. E., Medvedeva, G. I., Perova, N. B., & Shugarov, S. Yu. 1988, *General Catalogue of Variable Stars*, 4th Ed. (Moscow: Nauka) (GCVS)

Kraft, R. P., & Schmidt, M. 1963, ApJ, 137, 249

Kuijken, K., & Tremaine, S. 1994, ApJ, 421, 178

Landolt, A. U. 1992, AJ, 104, 340

Lasker, B. M., Sturch, C. R., McLean, B. J., Russell, J. L., & Jenkner, H. 1990, AJ, 99, 2019 (GSC)

Madore, B. F., & Freedman, W. L. 1991, PASP, 103, 933

McGonegal, R., McAlary, C. W., McLaren, R. A., & Madore, B. F. 1983, ApJ, 269, 641

Metzger, M. R., Caldwell, J. A. R., & Schechter, P. L. 1997, AJ, 115, in press (MCS)

Metzger, M. R., Tonry, J. L., & Luppino, G. A. 1993, in Astronomical Data Analysis Software and Systems II, eds. R. J. Hanisch, R. J. V. Brissenden, & J. Barnes, ASP Conf. Ser. 52, p. 300.

Pont, F., Mayor, M. & Burki, G. 1994, A&A, 285, 415

Schechter, P. L., Avruch, I. M., Caldwell, J. A. R., & Keane, M. J. 1992, AJ, 104, 1930

Schechter, P. L., Mateo, M., & Saha, A. 1993, PASP, 105, 1342

Schoening, B., Massey, P., Armandroff, T., Jacoby, G., Neese, C., & Salzer, J. 1991, *Operation of the CCD Direct Imaging Camera for the 0.9 Meter Telescope*, Kitt Peak National Observatory manual.

Welch, D. L., Wieland, F., McAlary, C. W., McGonegal, R., Madore, B. F., McLaren, R. A., & Neugebauer, G. 1984, ApJS, 54, 547

Table 1. Galactic Plane Regions, $50^\circ < \ell < 70^\circ$

Region	Center		J2000	
ID	ℓ°	b°	RA	Dec
01	60.09	-0.16	19 44 41.6	+23 53 26
02	59.91	0.16	19 43 06.8	+23 53 26
03	60.51	-0.16	19 45 36.5	+24 15 06
04	60.33	0.16	19 44 01.4	+24 15 06
05	60.92	-0.16	19 46 31.7	+24 36 45
06	60.74	0.16	19 44 56.3	+24 36 45
07	61.34	-0.16	19 47 27.2	+24 58 23
08	61.16	0.16	19 45 51.6	+24 58 23
09	61.76	-0.16	19 48 23.0	+25 20 00
10	61.58	0.16	19 46 47.1	+25 20 00
11	62.18	-0.16	19 49 19.2	+25 41 36
12	61.99	0.16	19 47 43.0	+25 41 36
13	62.59	-0.16	19 50 15.7	+26 03 10
14	62.41	0.16	19 48 39.2	+26 03 10
15	63.01	-0.16	19 51 12.5	+26 24 42
16	62.83	0.16	19 49 35.8	+26 24 42
17	63.43	-0.16	19 52 09.8	+26 46 14
18	63.25	0.16	19 50 32.7	+26 46 14
19	63.84	-0.16	19 53 07.3	+27 07 44
20	63.66	0.16	19 51 30.0	+27 07 44
21	64.26	-0.16	19 54 05.3	+27 29 12
22	64.08	0.16	19 52 27.6	+27 29 12
23	64.68	-0.16	19 55 03.6	+27 50 39
24	64.50	0.16	19 53 25.6	+27 50 39
25	65.09	-0.16	19 56 02.3	+28 12 04
26	64.91	0.16	19 54 24.0	+28 12 04
27	65.51	-0.16	19 57 01.5	+28 33 28
28	65.33	0.16	19 55 22.8	+28 33 28
29	65.93	-0.16	19 58 01.0	+28 54 50
30	65.75	0.16	19 56 22.0	+28 54 50
31	66.34	-0.16	19 59 00.9	+29 16 11
32	66.16	0.16	19 57 21.5	+29 16 11
33	66.76	-0.16	20 00 01.3	+29 37 30
34	66.58	0.16	19 58 21.6	+29 37 30
35	67.18	-0.16	20 01 02.0	+29 58 47
36	67.00	0.16	19 59 22.0	+29 58 47
37	67.60	-0.16	20 02 03.2	+30 20 02
38	67.42	0.16	20 00 22.8	+30 20 02
39	68.01	-0.16	20 03 04.9	+30 41 16
40	67.83	0.16	20 01 24.1	+30 41 16
41	68.43	-0.16	20 04 07.0	+31 02 28
42	68.25	0.16	20 02 25.9	+31 02 28
43	68.85	-0.16	20 05 09.6	+31 23 38
44	68.67	0.16	20 03 28.1	+31 23 38
45	69.26	-0.16	20 06 12.7	+31 44 46
46	69.08	0.16	20 04 30.7	+31 44 46
47	69.68	-0.16	20 07 16.2	+32 05 52
48	69.50	0.16	20 05 33.9	+32 05 52
49	70.10	-0.16	20 08 20.2	+32 26 56
50	69.92	0.16	20 06 37.5	+32 26 56

Table 1—*Continued*

Region	Center		J2000	
ID	ℓ°	b°	RA	Dec
51	59.67	-0.16	19 43 47.0	+23 31 44
52	59.49	0.16	19 42 12.5	+23 31 44
53	59.26	-0.16	19 42 52.8	+23 10 01
54	59.08	0.16	19 41 18.5	+23 10 01
55	58.84	-0.16	19 41 58.8	+22 48 17
56	58.66	0.16	19 40 24.8	+22 48 17
57	58.42	-0.16	19 41 05.1	+22 26 32
58	58.24	0.16	19 39 31.4	+22 26 32
59	58.01	-0.16	19 40 11.7	+22 04 46
60	57.82	0.16	19 38 38.2	+22 04 46
61	57.59	-0.16	19 39 18.6	+21 42 58
62	57.41	0.16	19 37 45.3	+21 42 58
63	57.17	-0.16	19 38 25.7	+21 21 10
64	56.99	0.16	19 36 52.7	+21 21 10
65	56.75	-0.16	19 37 33.2	+20 59 20
66	56.57	0.16	19 36 00.3	+20 59 20
67	56.34	-0.16	19 36 40.8	+20 37 30
68	56.16	0.16	19 35 08.2	+20 37 30
69	55.92	-0.16	19 35 48.7	+20 15 39
70	55.74	0.16	19 34 16.4	+20 15 39
71	55.50	-0.16	19 34 56.9	+19 53 46
72	55.32	0.16	19 33 24.7	+19 53 46
73	55.09	-0.16	19 34 05.3	+19 31 53
74	54.91	0.16	19 32 33.4	+19 31 53
75	54.67	-0.16	19 33 14.0	+19 09 59
76	54.49	0.16	19 31 42.2	+19 09 59
77	54.25	-0.16	19 32 22.8	+18 48 04
78	54.07	0.16	19 30 51.3	+18 48 04
79	53.84	-0.16	19 31 31.9	+18 26 08
80	53.66	0.16	19 30 00.6	+18 26 08
81	53.42	-0.16	19 30 41.2	+18 04 11
82	53.24	0.16	19 29 10.1	+18 04 11
83	53.00	-0.16	19 29 50.7	+17 42 13
84	52.82	0.16	19 28 19.8	+17 42 13
85	52.58	-0.16	19 29 00.5	+17 20 15
86	52.40	0.16	19 27 29.7	+17 20 15
87	52.17	-0.16	19 28 10.4	+16 58 16
88	51.99	0.16	19 26 39.8	+16 58 16
89	51.75	-0.16	19 27 20.5	+16 36 16
90	51.57	0.16	19 25 50.1	+16 36 16
91	51.33	-0.16	19 26 30.8	+16 14 15
92	51.15	0.16	19 25 00.6	+16 14 15
93	50.92	-0.16	19 25 41.4	+15 52 14
94	50.74	0.16	19 24 11.3	+15 52 14
95	50.50	-0.16	19 24 52.0	+15 30 12
96	50.32	0.16	19 23 22.1	+15 30 12
97	50.08	-0.16	19 24 02.9	+15 08 09
98	49.90	0.16	19 22 33.1	+15 08 09

Table 2. Observation Log

	Night							
	1	2	3	4	5	6	7	8
JD[a]	82	83	84	86	87	88	89	90
FWHM ″	1.4	1.4	2.5	2.0	1.7	2.2	1.8	1.4
Region	Filters Observed							
01	VI	I	I	I	VI		I	VI
02	I	I	I	I	VI		VI	VI
03	VI	I	I	I	VI		I	VI
04	VI	I	I	I	VI		I	VI
05	VI	I	I	I	VI		I	VI
06	VI	I	I	I	VI		I	VI
07	VI	I	I	I	VI		I	VI
08	VI	I	I	I	VI		I	VI
15	I		VI	I	VI	I	I	VI
16	I	I	VI	I	I	VI	I	VI
17	I	I	VI	I	I	I	VI	I
18	I	I	VI	I	I	I	VI	VI
19	I	I	VI	I	I	VI	I	VI
20	I	I	VI	I	I	VI	I	I
21	I	I	VI	I	I	VI	I	I
22	I	I	VI	I	I	VI	I	I
23	I	I	VI	I	I	VI	I	I
24	I	I	VI	I	I	VI	I	I
35	I	I	I	VI	I	I	VI	I
36	I	I	I	VI	I	I	VI	I
37	I	I	I	VI	I	I	VI	I
38	I	I	I	VI	I	I	VI	I
51	VI	I	I	I	VI		I	VI
52	VI	I	I	I	VI		I	VI
53	VI	I	I	I	VI		I	VI
54	VI	I	I	I	VI		I	VI
55	VI	I	I	I	VI		I	VI
56	VI	I	I	I	VI		I	VI
61	I	I	I	VI	I		VI	I
62	I	I	I	VI	I		VI	I
63	I	I	I	VI	I		VI	I
64	I	I	I	VI	I		VI	I
65	I	I	I	VI	I		VI	I
66	I	I	I	VI	I		VI	I
75		I	I	I	I	I	VI	I
76		I	I	VI	I	I	VI	I
77			I	VI	I	I	VI	I
78			I	VI	VI	I	VI	I
81	I	I	I	VI	I	VI	I	VI
82	I	I	I	VI	I	VI	I	VI
83	I	I	I	VI	I	VI	I	VI
84	VI	I	I	VI	I	VI	I	VI

[a] Julian date minus 2,448,700

Table 3. High Amplitude Variable Stars

Catalog ID	RA (J2000)	Dec	$\langle I \rangle$	σ_I	χ^2_ν	$\langle V \rangle - \langle I \rangle$	Notes
01-00195	19 44 48.0	+23 54 18	15.20	0.084	59.6	1.88	
01-00427	19 44 24.8	+23 49 51	17.88	0.596	44.8		
01-00637	19 44 44.6	+23 53 35	16.20	0.206	31.2		1
01-00793	19 44 21.4	+23 47 42	16.03	0.087	28.3	1.78	
01-00966	19 45 00.3	+23 56 22	16.90	0.108	15.0	2.76	
01-01196	19 44 52.2	+23 52 04	16.84	0.233	24.3	2.95	
01-03774	19 45 13.3	+23 50 03	13.42	0.152	185.9	1.62	
01-05204	19 44 45.2	+23 44 40	17.69	0.559	34.6		
01-07279	19 44 33.4	+23 46 52	17.48	0.167	16.0		
01-08549	19 44 58.9	+23 59 47	12.40	0.123	203.7	3.35	1
01-08687	19 45 13.6	+23 59 35	14.09	0.076	43.1	1.44	
01-09100	19 45 25.3	+23 54 50	16.11	0.061	14.7	1.99	
01-09318	19 45 15.7	+24 00 51	16.42	0.080	16.5	2.19	
01-11655	19 44 08.9	+23 56 58	15.07	0.099	52.7	1.69	
01-11809	19 43 52.7	+24 04 34	16.07	0.124	17.6		
01-11982	19 44 23.6	+23 59 47	17.20	0.136	12.6		
01-12561	19 43 49.8	+23 56 50	16.09	0.634	373.2	2.03	
01-19057	19 43 59.8	+24 05 03	15.00	0.240	21.7		
02-00285	19 43 01.1	+23 47 31	15.40	0.149	75.9	1.96	
02-02092	19 42 42.7	+23 47 38	18.48	0.553	22.9		
02-02141	19 43 02.3	+23 45 16	13.63	0.249	667.7	1.08	
02-02434	19 43 09.5	+23 47 06	16.17	0.080	17.8	2.56	2
02-02442	19 43 41.1	+23 46 54	16.08	0.150	47.7	2.10	
02-02735	19 43 47.6	+23 54 22	17.44	0.218	19.4	2.39	
02-04392	19 42 26.5	+23 44 02	16.88	0.164	25.5	2.35	
02-05822	19 43 21.4	+24 02 06	15.21	0.066	32.6	1.75	
02-06335	19 43 22.3	+23 59 45	16.51	0.123	22.3	2.38	
02-06414	19 43 46.0	+23 54 56	16.51	0.187	64.4	2.44	
02-07921	19 42 33.4	+24 01 06	15.20	0.114	11.5	1.71	
03-00022	19 46 01.7	+24 14 22	12.62	0.442	2763.6	1.12	
03-00055	19 45 51.7	+24 09 11	12.96	0.094	22.8	2.81	
03-00092	19 45 36.7	+24 12 09	13.21	0.087	67.6	3.20	1
03-00360	19 45 27.6	+24 11 39	15.55	0.175	99.1	1.71	
03-00433	19 45 21.1	+24 20 06	15.43	0.100	13.5	1.65	
03-02298	19 45 42.8	+24 11 36	17.50	0.300	17.6	2.21	
03-02725	19 45 24.0	+24 19 34	17.88	0.752	25.8	1.16	
03-06544	19 46 11.5	+24 09 04	12.51	0.090	77.1	2.72	1
03-06552	19 46 04.0	+24 05 36	12.06	0.252	757.2	2.36	
03-12117	19 45 03.6	+24 04 16	15.25	0.147	47.0	2.70	2
03-12186	19 44 45.5	+24 12 58	15.64	0.090	15.9	1.58	
03-12425	19 45 07.2	+24 04 07	16.11	0.082	13.5	2.85	
03-13446	19 45 09.4	+24 09 24	17.94	0.201	16.3		
03-15534	19 45 36.9	+24 26 15	13.78	0.092	15.2		
03-15889	19 45 55.4	+24 24 48	16.39	0.292	61.0	2.99	
03-15979	19 45 40.3	+24 21 52	16.33	0.130	24.1	2.04	
03-15994	19 46 15.6	+24 21 27	15.58	0.119	47.1	2.08	
03-17215	19 46 11.6	+24 21 58	17.76	0.307	18.4	1.94	
04-00354	19 43 49.9	+24 13 30	15.47	0.164	138.1	2.76	
04-01038	19 44 17.4	+24 17 55	16.98	0.187	21.1	1.66	
04-01192	19 44 02.1	+24 15 32	17.06	0.264	25.8	2.50	...

Table 4. New Cepheids

Star	Catalog ID	RA (J2000)	Dec	$\langle I \rangle$	$\langle V \rangle$–$\langle I \rangle$	Period
19313+1901	76-13269	19 31 15.5	+19 00 42	15.54	4.3	4.1643
19430+2326	52-04808	19 42 59.5	+23 25 35	13.37	4.7	7.8888
19431+2305	53-00371	19 43 07.3	+23 04 33	16.06	> 6	5.6646
19456+2412	03-00092	19 45 36.7	+24 12 09	13.21	3.2	4.0758
19504+2652	18-00380	19 50 26.0	+26 51 44	16.09	5.2	5.8326
19508+2620	15-00026	19 50 49.3	+26 19 45	12.85	3.8	5.9497
19462+2409	03-06544	19 46 11.5	+24 09 04	12.51	3.0	3.8799
19462+2501	08-00258	19 46 11.9	+25 00 33	15.28	3.7	4.7842
19468+2447	07-11383	19 46 46.9	+24 46 47	11.43	2.7	4.9427
20010+3011	38-09441	20 01 01.4	+30 11 17	13.91	3.8	7.1395
19286+1733	84-01800	19 28 37.7	+17 32 36	12.24	1.9	4.1643

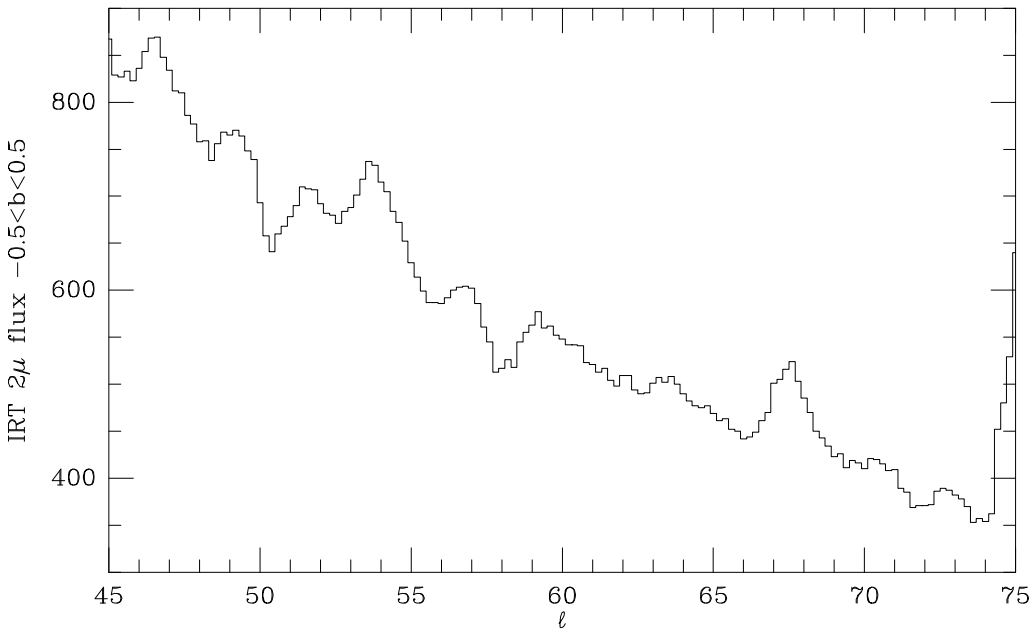

Fig. 1.— Spacelab IRT flux in the Galactic plane, integrated over one degree in latitude (raw data provided by S. Kent). The flux units are arbitrary. A general trend as a function of longitude can be seen along with smaller-scale variations. The effective resolution is about 1 degree; some peaks may be due to strong unresolved point sources. Note the strong peaks near $\ell = 68^\circ$ and $\ell = 54^\circ$, and the low brightness near $\ell = 58^\circ$.

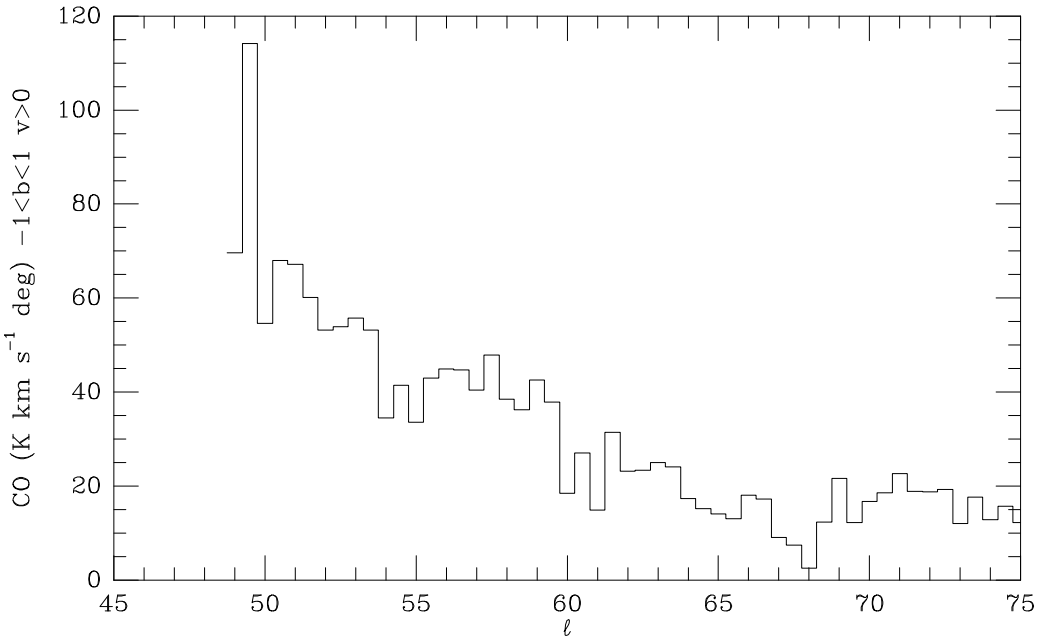

Fig. 2.— Galactic CO emission integrated over $|b| < 1°$, including only gas with positive velocities with respect to the LSR. Note the similarity of the features between this map and the 2μ map, inverted, so that high 2μ corresponds to low CO emission as is expected if the features are caused by differential extinction.

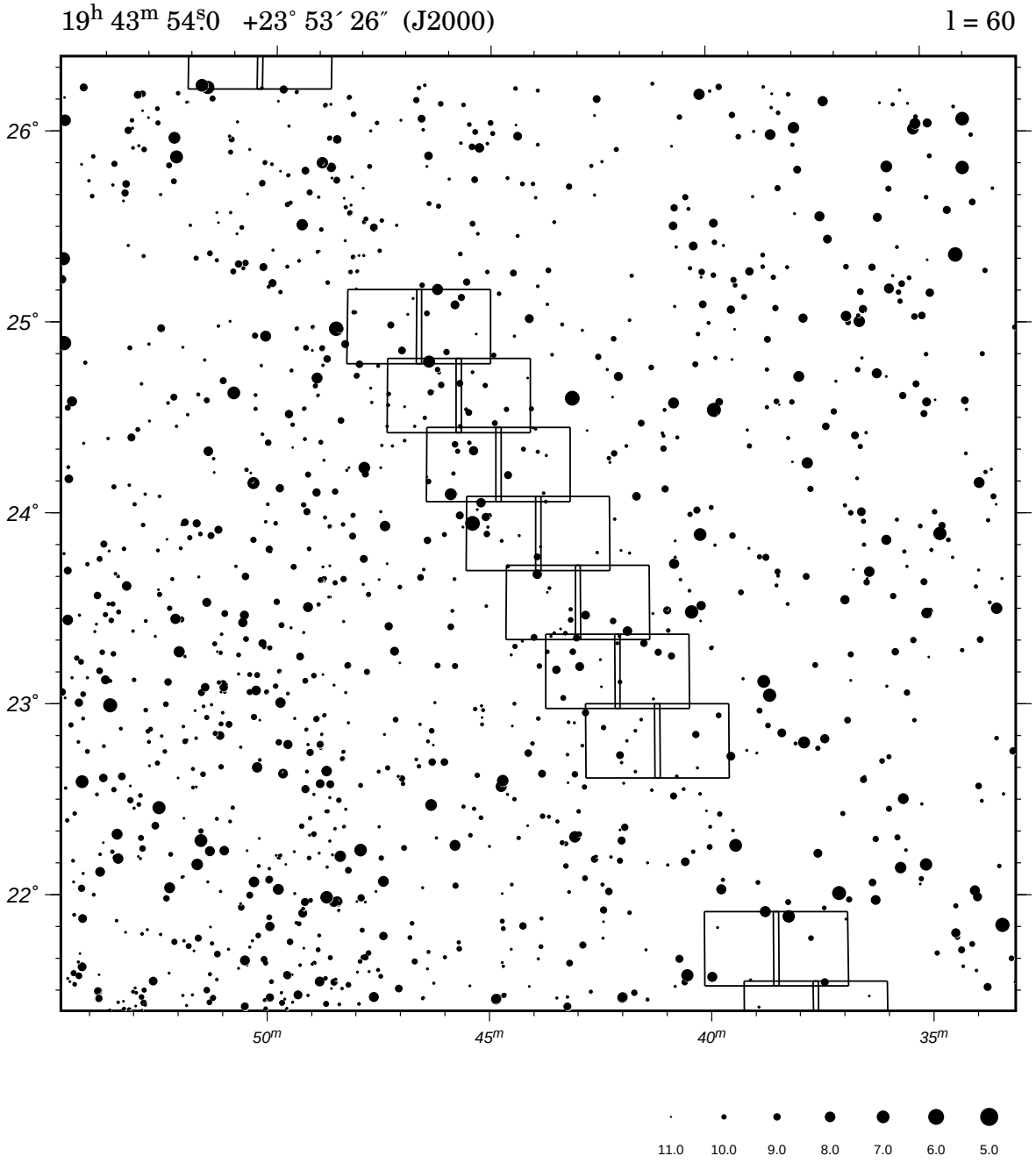

Fig. 3.— A chart made using data from the HST Guide Star Catalog, showing catalog stars brighter than V= 11 in a 5 degree square region centered on $\ell = 60°, b = 0°$. Regions observed in the Cepheid survey are outlined. The index in the lower right corner shows the point size scale for V magnitudes.

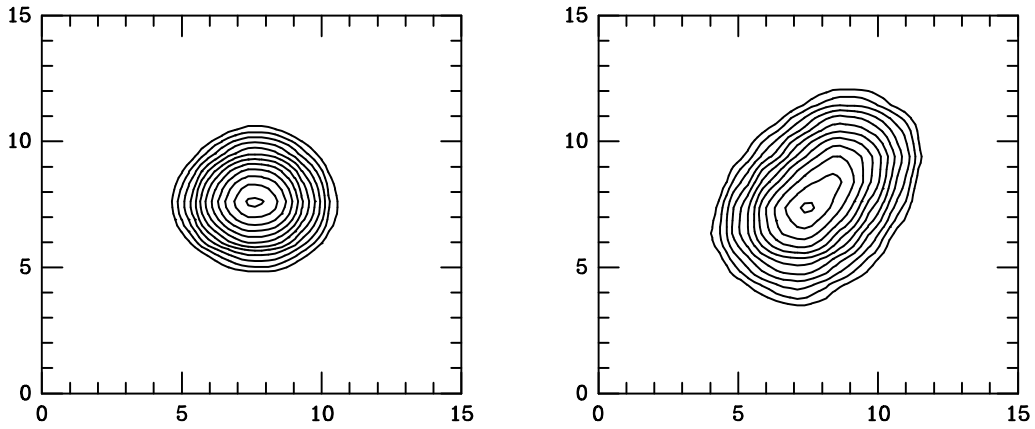

Fig. 4.— Stellar point-spread intensity functions at the center (left panel) and corner (right panel) of the CCD in a single exposure. The inside contour is chosen near the peak, and subsequent contours are spaced logarithmically by factors of $\sqrt{2}$. The image was taken in a period of relatively good seeing (1.″5). Axes are shown in units of pixels; the boxy appearance is an artifact of the reconstruction.

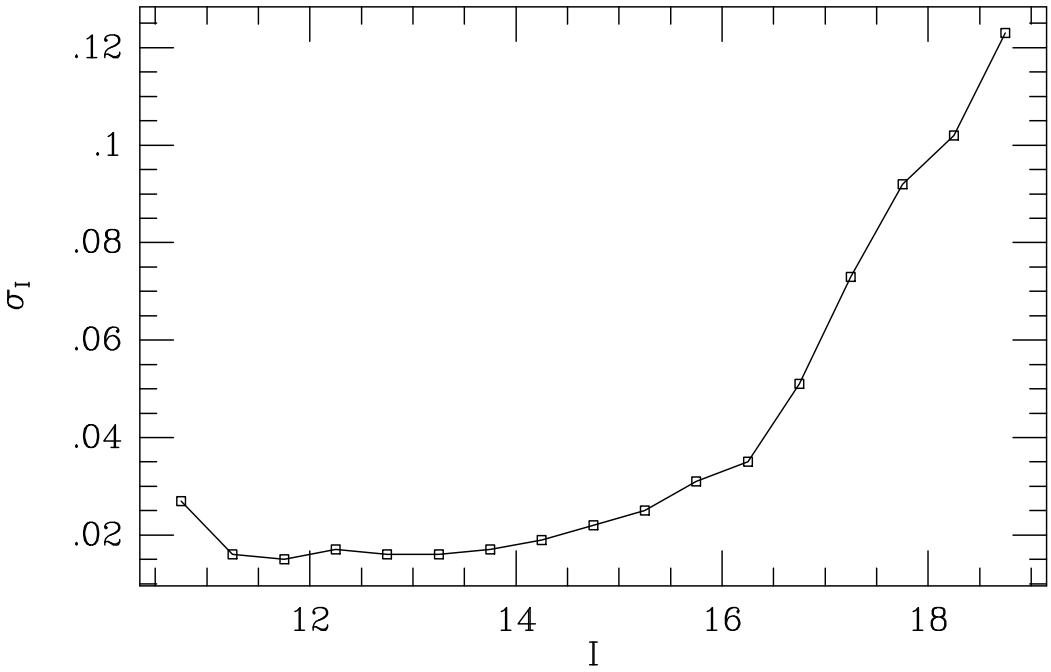

Fig. 5.— Measured dispersion in magnitudes for survey stars, plotted as a function of I magnitude.

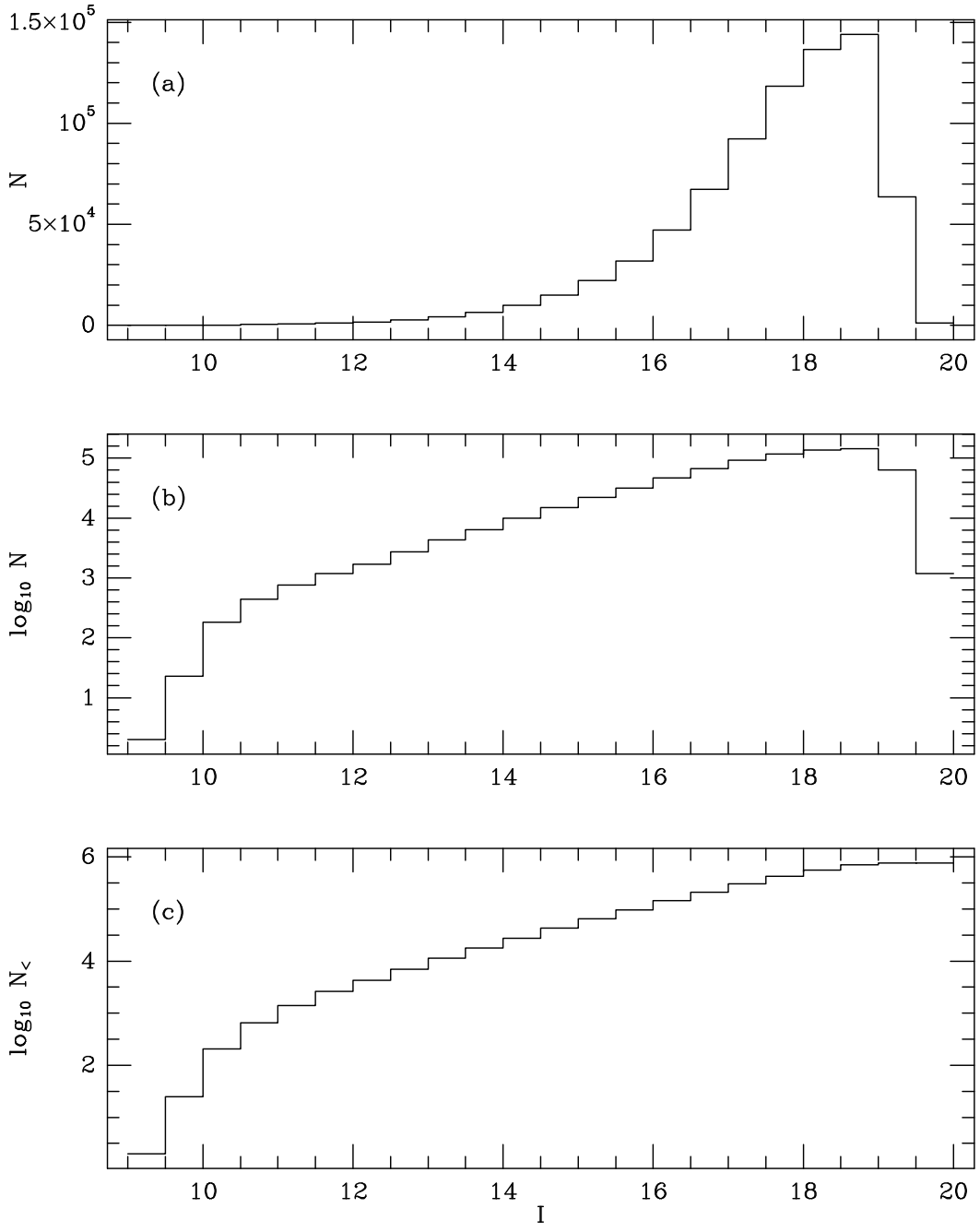

Fig. 6.— The magnitude distribution for stars in the survey, counted in 0.5 magnitude bins. (a) The linear count distribution as a function of apparent I magnitude. Only objects detected on multiple nights are included. (b) Same counts as (a) on a logarithmic scale. (c) The cumulative count distribution. The bright and faint magnitude cutoffs are evident; between the two the distribution follows roughly a power law in flux, though the exponent decreases slightly with fainter magnitude. $d\log N/dI \simeq 0.38$ at $I = 14$.

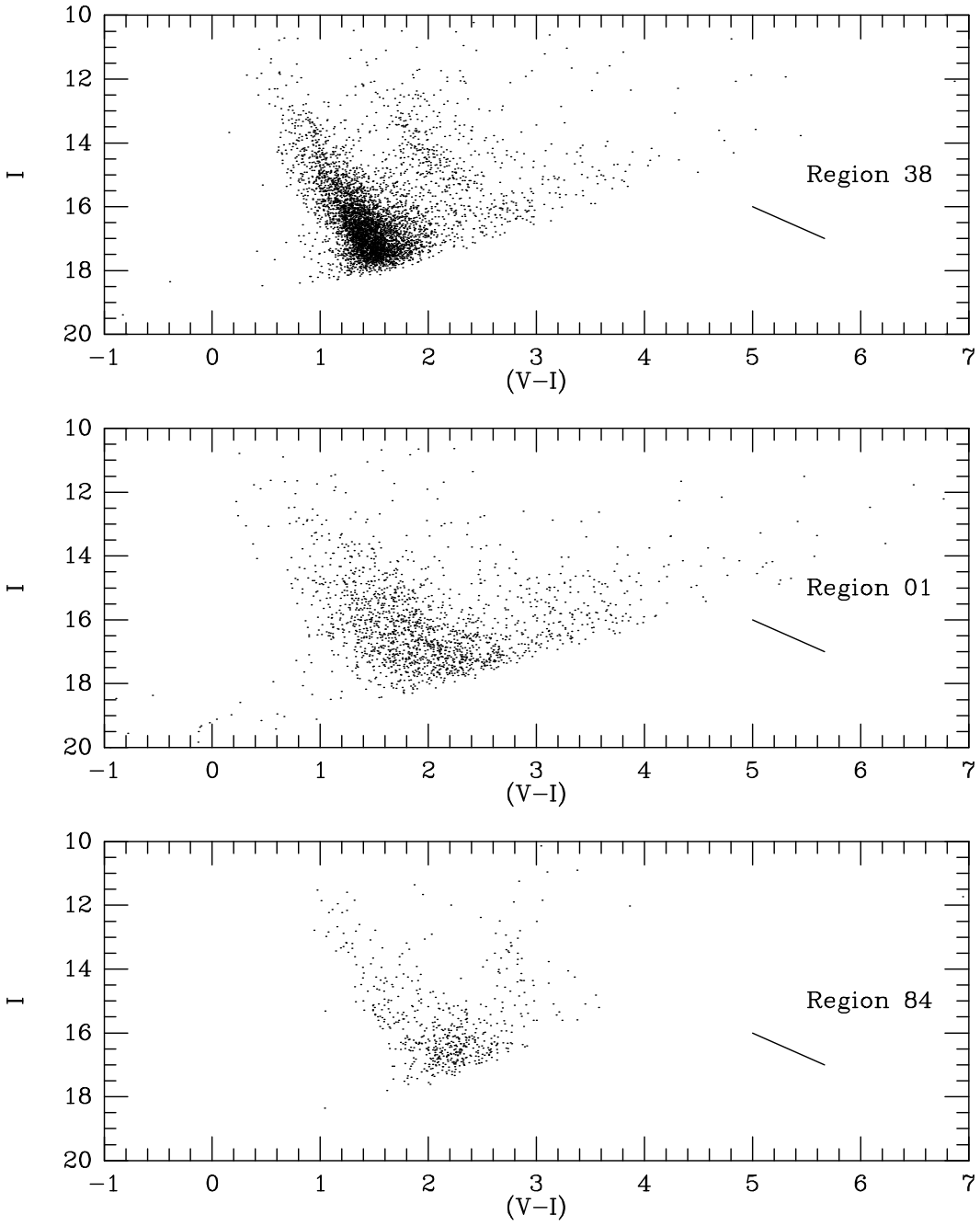

Fig. 7.— Color-magnitude diagrams for three survey regions: Region 38 at $\ell = 67.5°$, Region 1 at $\ell = 60°$, and Region 84 at $\ell = 52.9°$. To reduce crowding, one-thrid of the stars with (V–I) colors are plotted for each region. The line at the lower right of each plot shows the reddening vector for $A_V = 1$.

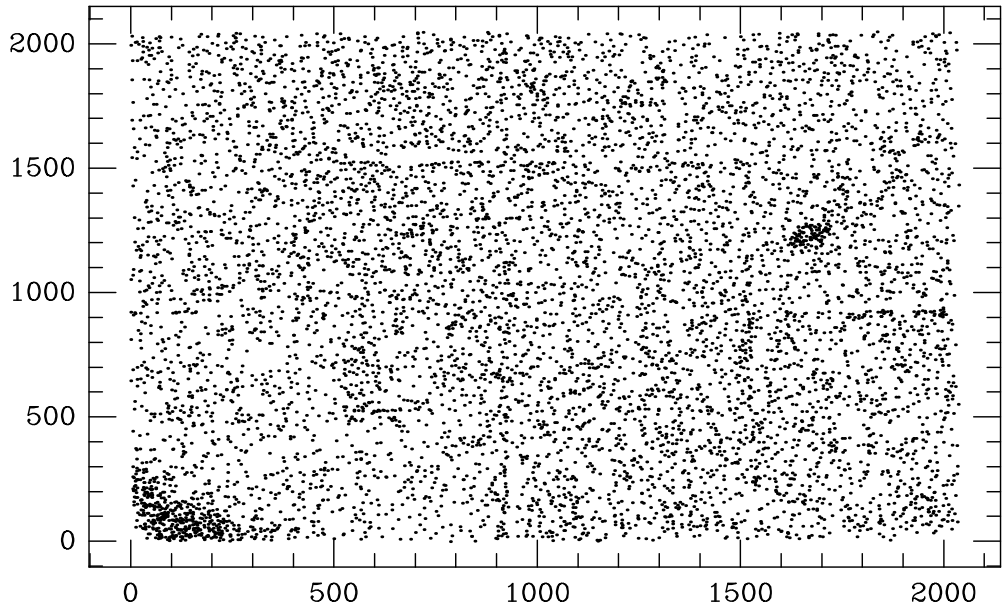

Fig. 8.— Pixel coordinates on the detector for the 7,821 survey stars flagged as variable. Two regions of significant excess can be seen, one in the corner where the point spread function was highly elongated, and the other near (1700,1200) where the detector response may have been nonlinear. Some signs of the tiling procedure are also evident.

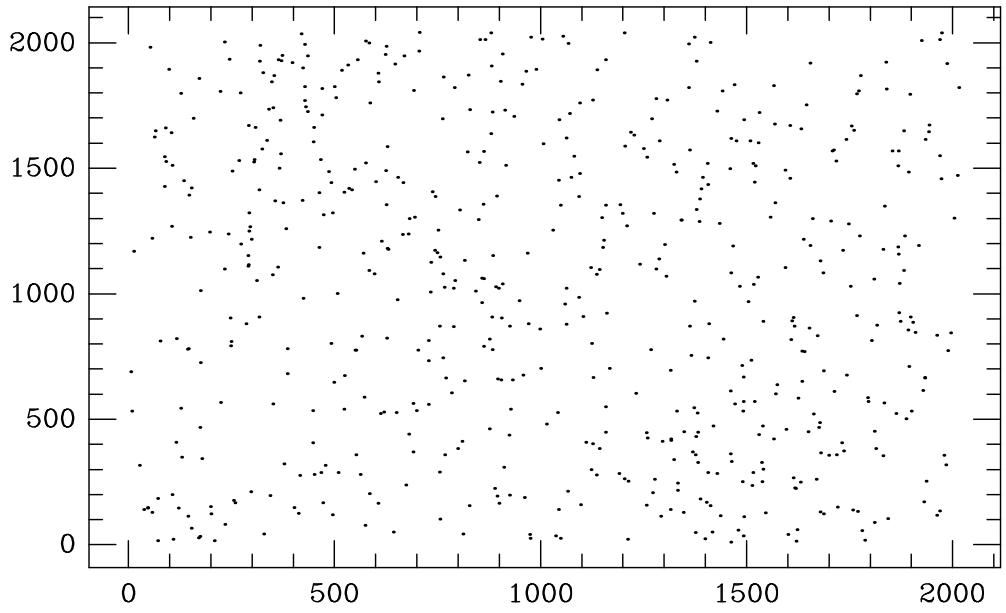

Fig. 9.— Detector pixel coordinates of 578 Cepheid candidates.

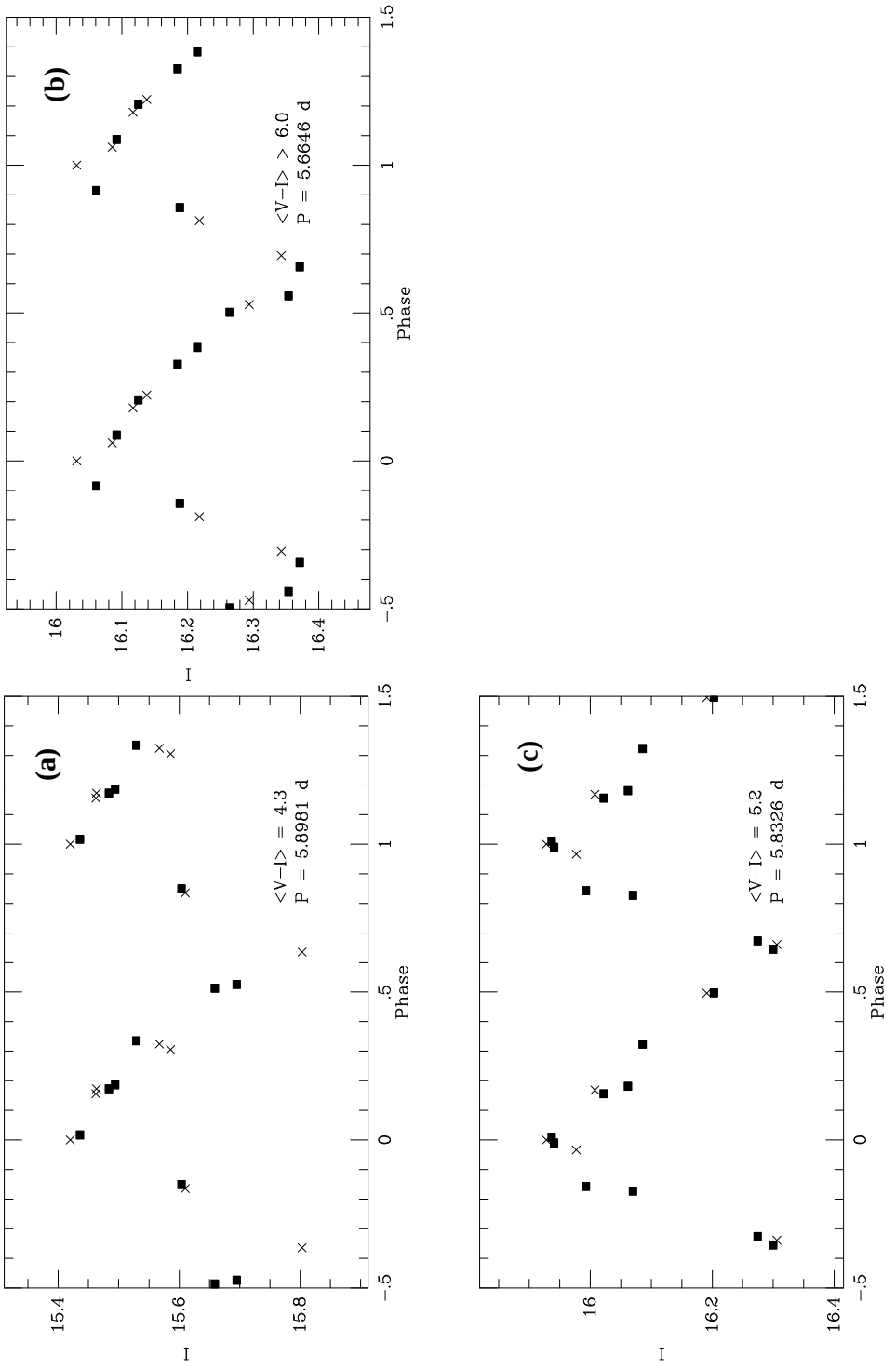

Fig. 10.— I light curve for the Cepheids (a) 19313+1901; (b) 19431+2305; and (c) 19504+2652. Crosses are data from the 1992 survey, squares from the 1993 followup. These three Cepheids were too faint in the survey data for an accurate measurement of the dV/dI slope.

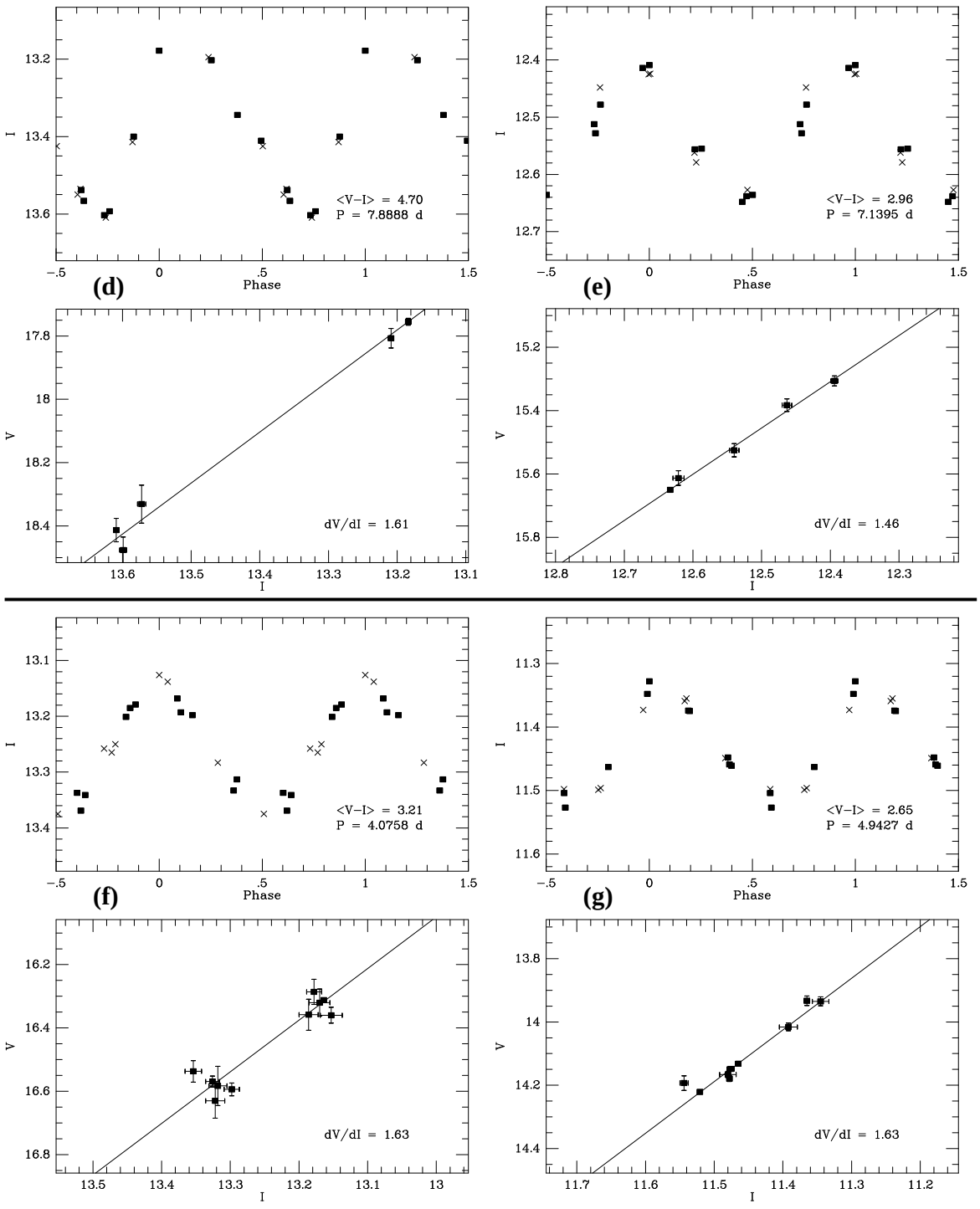

Fig. 11.— I light curve and two-band plot for the Cepheids (d) 19430+2326; (e) 19462+2409; (f) 19456+2412; and (g) 19468+2447.

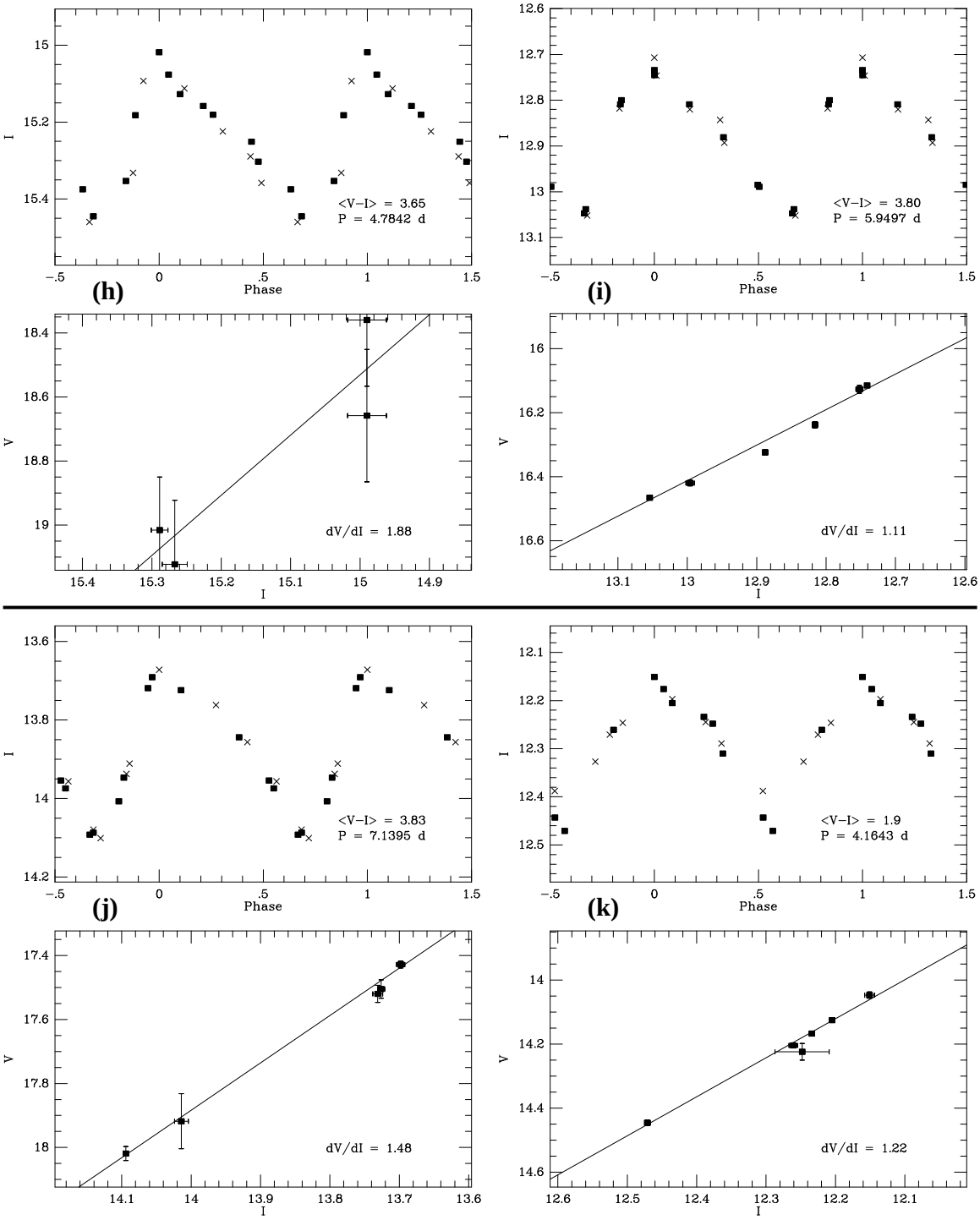

Fig. 12.— I light curve and two-band plot for Cepheids (h) 19462+2501; (i) 19508+2620; and (j) 20010+3011. Panel (k) shows the possible Cepheid 19286+1733.

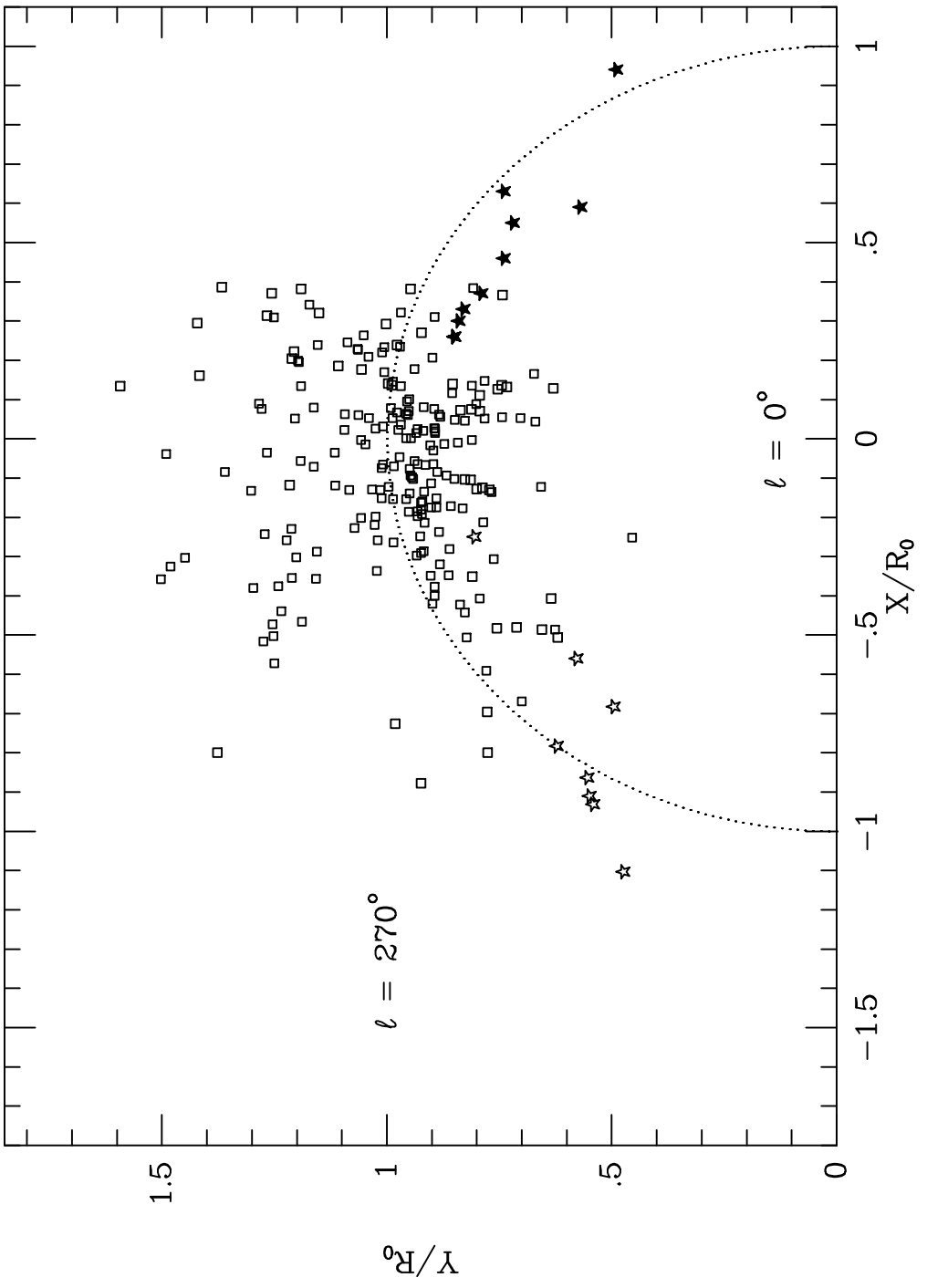

Fig. 13.— Locations of Cepheids in the Milky Way disk, plotted with open squares. Open stars show Cepheids discovered by CKS in a southern hemisphere survey; newly discovered northern hemisphere Cepheids from this paper are shown as filled stars. Cartesian coordinates are shown in units of R_0 with the Galactic center at (0,0) and the Sun at (0,1); the solar circle ($R = R_0$) is indicated by a dotted line.